Ocean color remote sensing of seagrass and bathymetry in the Bahamas Banks by high-resolution airborne imagery

Heidi M. Dierssen and Richard C. Zimmerman

Moss Landing Marine Laboratories, California State University, 8272 Moss Landing Road, Moss Landing, California 95039

Robert A. Leathers, T. Valerie Downes, and Curtiss O. Davis

Naval Research Laboratory, Code 7212, 4555 Overlook Avenue SW, Washington, D.C. 20375

Abstract

New coastal ocean remote sensing techniques permit benthic habitats to be explored with higher resolution than ever before. A mechanistic radiative transfer approach is developed that first removes the distorting influence of the water column on the remotely sensed signal to retrieve an estimate of the reflectance at the seafloor. The retrieved bottom reflectance is then used to classify the benthos. This spectrally based approach is advantageous because model components are separate and can be evaluated and modified individually for different environments. Here, we applied our approach to quantitatively estimate shallow-water bathymetry and leaf area index (LAI) of the seagrass *Thalassia testudinum* for a study site near Lee Stocking Island, Bahamas. Two high-resolution images were obtained from the ocean portable hyperspectral imager for low-light spectroscopy (Ocean PHILLS) over the study site in May 1999 and 2000. A combination of in situ observations of seafloor reflectance and radiative transfer modeling was used to develop and test our algorithm. Bathymetry was mapped to meter-scale resolution using a site-specific relationship ($r^2 = 0.97$) derived from spectral ratios of remote sensing reflectance at 555 and 670 nm. Depth-independent bottom reflectance was retrieved from remote sensing reflectance using bathymetry and tables of modeled water column attenuation coefficients. The magnitude of retrieved bottom reflectance was highly correlated to seagrass LAI measured from diver surveys at seven stations within the image ($r^2 = 0.88$–0.98). Mapped turtlegrass LAI was remarkably stable over a 2-yr period at our study site, even though Hurricane Floyd swept over the study site in September 1999.

Managing and preserving coastal marine resources is a formidable challenge given the rapid pace of change affecting coastal environments. Fast, accurate, and quantitative tools are needed for detecting change in coastal ecosystems. Traditional in situ surveys are time and labor intensive, generally lack the spatial resolution and precision required to detect subtle changes before they become catastrophic, and can be difficult to maintain from year to year (Orth and Moore 1983; Peterson and Fourqurean 2001). Aerial photography provides more effective spatial coverage and has been used to semiquantitatively map benthic substrates (Ferguson et al. 1993; Kirkman 1996; Sheppard et al. 1995), but it is not effective at distinguishing color differences due to variations in water depth. The spectral reflectance obtained from digital remote sensing imagery represents a considerable advancement over conventional photography and allows for physically based analyses using inherent spectral signatures (Campbell 1996).

Techniques for using remote sensing imagery to map benthic vegetation are still in their infancy. Unsupervised classification is frequently used as a means for identifying features within a discrete image but does not provide mathematical algorithms that can be extrapolated to other images and regions. In addition, the optical signal coming from the benthic vegetation is strongly modulated by the effects of the overlying water column. Unsupervised classification techniques neglect the confounding effects of reflectance from the benthos and spectral shifts due to the water column and can lead to significant errors. Therefore, accurate assessments of the water depth and inherent optical properties of the water column must be considered in quantitative interpretations of imagery from optically shallow waters.

A commonly used approach is to create indices from the remotely sensed bands that are independent of water depth (Lyzenga 1978, 1981). The correction presented by Lyzenga (1981) assumes that the upwelling radiance is exponentially dependent on the water depth and can be approximated by the downwelling diffuse attenuation coefficient. The seafloor, however, changes the angular distribution of the reflected light field and serves as a reflective source of upwelling photons. Thus, upwelling radiance in optically shallow water cannot be represented by a simple exponential decay function. Its attenuation coefficient is frequently different from the downwelling irradiance attenuation and should be con-
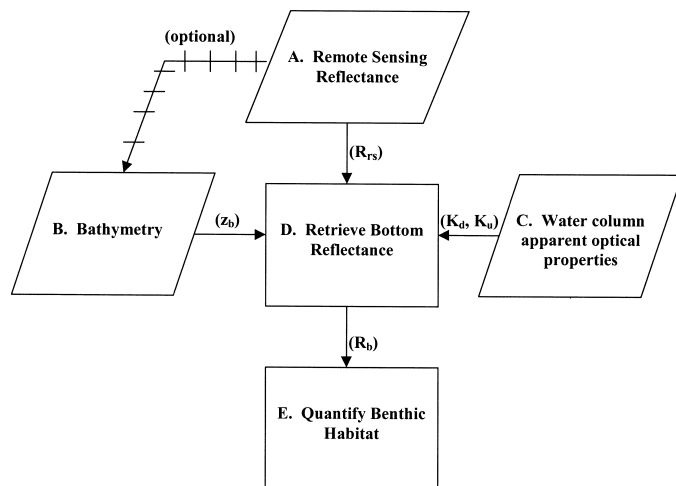
Fig. 1. Flowchart outlining the general approach used to quantify the benthic habitat from remote sensing reflectance. The steps are ordered (A–E) following the sequence in which they are presented in the Results.

sidered in the context of the water depth and bottom albedo (Maritorena et al. 1994). Additionally, these bottom indices are composites of spectral data that incorporate water column attenuation. Changes in water column attenuation coefficients will modify these indices and, more importantly, the algorithms used to quantify the benthos. Hence, the use of depth-invariant bottom indices might require extensive recalibration for each application.

Another method for evaluating water column effects on remotely sensed spectra is to use radiative transfer theory to propagate bottom-reflected light through different depths of water column for a given set of water column optical properties. The resulting spectral library represents a database of different bottom types (endmembers) and depths that can then be matched to the remote sensing spectra. The spectral library approach can be effective (Louchard et al. 2003), especially if the endmembers are significantly different, but it is computationally and labor intensive. Furthermore, all of the radiative transfer simulations must be redone for each endmember and bottom depth when the optical properties of the water column change. Because this approach compares both the magnitude and shape of the remote sensing spectra to the modeled spectral library, the input conditions to the radiative transfer model (e.g., sky conditions, water column inherent optical properties, particle phase functions) must be accurate in order to closely approximate the measured spectra.

The objective of this study was to present an alternative approach to quantifying benthic habitats from remote sensing imagery. Our general approach (Fig. 1) was to retrieve bottom reflectance from remotely sensed reflectance measured above the sea surface and use this retrieved bottom reflectance to quantify the benthos. The advantage of this spectrally based approach is that model components are separate and can be evaluated and modified individually for different environments. Here, we applied this approach to estimate leaf area index (LAI) of the seagrass *Thalassia testudinum* (turtlegrass) from high-resolution hyperspectral im-

agery collected around Lee Stocking Island, Bahamas. Seagrass meadows represent important structural and biogeochemical components of estuarine and coastal environments throughout the world (Hemminga and Duarte 2000). Because of their vulnerability to anthropogenic degradation of coastal environments (Orth 1977; Cambridge and McComb 1984; Zieman et al. 1988; Valiela et al. 1992), remote sensing methods are needed to rapidly and accurately evaluate the expansion or decline of seagrass populations.

The remote sensing algorithm presented here was developed and tested against in situ observations of seafloor reflectance and remote sensing reflectance at the sea surface. Because our approach requires only a handful of radiative transfer simulations, it can be rapidly modified to account for changes in water column optical properties. In addition, the specific relationships incorporated into this algorithm were focused on spectral bands that coincide with multichannel ocean color sensors (e.g., sea-viewing wide field-of-view sensor [SeaWiFS] and moderate-resolution imaging spectroradiometer [MODIS]); therefore, the algorithm might be portable to multispectral imagery spanning larger regional areas.

Methods

Study site—The test site selected for evaluating our algorithm was located on the shallow banks around Lee Stocking Island, Bahamas ($23°46.4'$N, $76°6.4'$W), with the Caribbean Marine Research Center as a base of operation (Fig. 2). Our study site between Lee Stocking Island and Norman's Pond Cay was located in a tidal channel through which water flowed between the shallow Bahamas Bank and the deep waters of Exuma Sound. A migrating high-energy dune field composed of ooitic carbonate sand occupies the center of the channel where tidal flows can exceed 1 m s^{-1}. The substrate east of the high-energy dune field is vegetated by a virtually monotypic stand of turtlegrass (*Thalassia testudinum*), with occasional manateegrass (*Syringodium filiforme*) interspersed among the turtlegrass nearshore. The sediment consists of coarse carbonate sand and identifiable leaf litter, particularly where turtlegrass densities are high.

Field data—A variety of field measurements were taken in May 1999 and 2000 to evaluate optical closure in these clear waters and to develop remote sensing algorithms. A hyperspectral tethered spectral radiometer buoy, HTSRB (Satlantic), was used to measure downwelling spectral irradiance (E_d) above the sea surface (395–795 nm, 2.5-nm bandwidth), upwelling spectral radiance (L_u) at 0.65 m below the sea surface, and acoustic depth (Table 1). The HTSRB was deployed at specific stations in conjunction with diver measurements of seagrass densities and bottom reflectance. The resulting station data were used to develop the LAI algorithm. The HTSRB was also towed along a series of transects throughout the large study area (~10 km, Fig. 2C). Position was recorded with a differential GPS receiver interfaced to the HTSRB control software. These transect data were used to develop the bathymetry algorithm. Spectral data were interpolated to 5 nm with a cubic spline. Spectral L_u (measured 0.65 m beneath the sea surface) was extrapo-
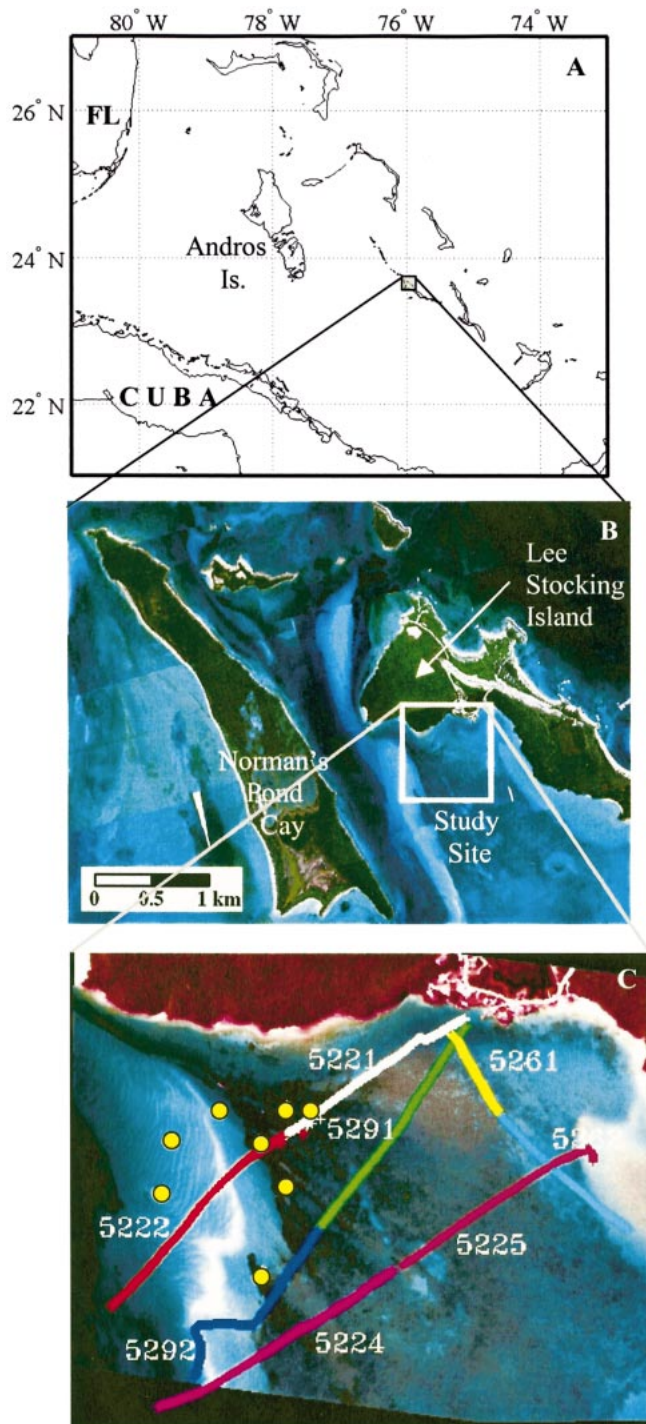
Dierssen et al.

Fig. 2. (A) Location of Lee Stocking Island along the Exuma Islands chain, Bahamas. (B) A composite PHILLS true-color image of Lee Stocking Island and the study site from June 1999. (C) Location of sampling stations for seagrass LAI, R_b, and R_{rs} (yellow circles) and numbered HTSRB transects (colored lines) within the study site image.

Table 1. Definitions of abbreviations and acronyms.

Symbol	Definition
DOBBS	Diver-operated benthic bio-optical spectrometer
E_d	Spectral downwelling plane irradiance (W m^{-2} nm^{-1})
E_u	Spectral upwelling plane irradiance (W m^{-2} nm^{-1})
HTSRB	Hyperspectral tethered spectral radiometer buoy
K	Operational attenuation coefficient representing attenuation of both the downwelling and upwelling streams
K_d	Attenuation coefficient of downwelling irradiance E_d (m^{-1})
$\bar{K}_{Lu}$	Depth-averaged attenuation coefficient of upwelling radiance L_u (m^{-1})
LAI	Leaf area index (m^2 leaf m^{-2} seafloor)
L_u	Spectral upwelling radiance (W m^{-2} sr^{-1} nm^{-1})
L_w	Spectral water-leaving radiance (W m^{-2} sr^{-1} nm^{-1})
MODIS	Moderate-resolution imaging spectroradiometer
PHILLS	Ocean portable hyperspectral imager for low-light spectroscopy
Q	Q factor [E_u/L_u] just beneath the sea surface (sr)
Q_b	Q factor [E_u/L_u] at the seafloor (sr)
R_b	Irradiance reflectance [$E_u E_d$] at the seafloor
R_{rs}	Remote sensing reflectance [L_w/E_d] (sr^{-1})
R_∞	Irradiance reflectance just beneath the sea surface measured over an infinite water column
SeaWiFS	Sea-viewing wide field-of-view sensor
t	Transmittance of upwelling radiance and downwelling irradiance across the air–water interface
z_b	Bottom depth (m)

the seafloor at each station with the diver-operated benthic bio-optical spectrometer (DOBBS), a three-channel HydroRad (HOBI Labs) modified for portable, in situ operation by a diver. Each channel of the DOBBS was fitted with a cosine collector to measure plane irradiance across the photosynthetically active spectrum (0.3-nm resolution, 400–700 nm). Spectral data were interpolated to 1 nm with a cubic spline and smoothed with a 20-nm running average. Bottom reflectance, R_b, was calculated as the ratio of E_u to E_d measured within centimeters of the substrate (bare sand or top of turtlegrass canopy). We only present DOBBS data from 450 to 650 nm because of signal-to-noise problems with the instrument at both ends of the spectrum.

Turtlegrass shoot density was estimated at each station with 15–20 randomly located quadrats. The seven stations were selected to span a range of turtlegrass densities from sparse (LAI < 0.5) to dense (LAI > 2) canopies. One shoot was collected haphazardly from each quadrat and the length (nearest 1 mm) and width (nearest 0.01 mm) of each leaf was measured in the laboratory. LAI was estimated from leaf morphometrics and shoot density counts as the average one-sided leaf area per square meter of substrate.

Reflectance of individual turtlegrass leaves were measured in the laboratory with a Shimadzu UV2101PC scanning spectrophotometer fitted with an integrating sphere. Sand reflectance was measured with an Ocean Optics S2000 spectrophotometer (Louchard et al. 2003).

Radiative transfer modeling—We utilized the radiative transfer model, Hydrolight (Sequoia Scientific; Mobley

lated to water-leaving radiance (L_w) with a radiative transfer model, as described below. Remote sensing reflectance (R_{rs}) was estimated as the ratio of L_w to E_d and adjusted for instrument self-shading effects (Leathers et al. 2001a).

Both upwelling irradiance (E_u) and E_d were measured near

1994), to estimate the downward and upward diffuse attenuation coefficients, K_d and K_{Lu}, within the water column. These coefficients describe the attenuation of E_d and L_u, respectively, and depend on the inherent optical properties of water, water depth, bottom type, and illumination conditions. Inputs into Hydrolight included the mean absorption and attenuation coefficients measured in these waters with a Wetlabs *ac*-9, the average Petzold particle scattering phase function, a semiempirical sky model based on date and time of day (Gregg and Carder 1990), and a wind speed of 5 m s⁻¹. Raman scattering effects were included in all model runs. Hydrolight was parameterized using water depths ranging from 1 to 10 m and bottom types comprised of turtlegrass and sand. The water column was assumed to be homogeneous and a mean set of attenuation coefficients was used to represent the water column for both years. The bottom reflectances input in Hydrolight were those measured for the pure components in the laboratory, as described above. Hydrolight computes vertical profiles of L_u and E_d, from which the diffuse attenuation coefficients can be computed. The depth-averaged $\bar{K}_{Lu}(z_b)$ was calculated for each bottom depth, z_b, as the attenuation occurring between the radiance estimated just beneath the sea surface, $L_u(0^-)$, and that estimated just above the seafloor, $L_u(z_b)$.

$$\bar{K}_{Lu}(z_b) = \frac{1}{z_b}\log\left(\frac{L_u(0^-)}{L_u(z_b)}\right) \tag{1}$$

Remote sensing data—Aerial remote sensing data were obtained over Lee Stocking Island in 1999 and 2000 with the ocean portable hyperspectral imager for low-light spectroscopy (Ocean PHILLS) airborne sensor, an imaging spectrometer specifically designed for coastal waters (Davis et al. 2002). The imagery, taken from an Antonov biplane flown at 2,600 m, contains 1024 across-track samples and 128 spectral channels between 380 and 1,000 nm.

Spectral calibration of the PHILLS was accomplished by imaging several different gas lamps (oxygen, mercury, argon, helium) and identifying the locations of known gas emission lines. This spectral calibration was fine-tuned after each deployment by identifying strong atmospheric absorption features in the field data. The radiometric calibration was performed with a Spectraflect-coated integrating sphere (Labsphere) containing 10 halogen lamps. The intensity of the sphere at each lamp level was determined by performing a transfer calibration from a lamp calibrated by the National Institute of Standards and Technology. Because the spectrum of the source lamps was much more intense at red wavelengths than at blue wavelengths, a blue balancing filter was placed in front of the PHILLS lens to flatten the source illumination spectrum. For the 1999 data presented here, blue-filtered calibration data for 0, 1, 2, 3, 4, 6, 8, and 10 illuminated lamps were used to acquire a quadratic relationship between data counts and radiance for each pixel on the array. For the 2000 data, a linear calibration was performed with data from 0, 1, 2, and 3 unfiltered calibration lamps.

Two images of the study site were selected for analysis, one from 31 May 1999 (PHILLS 99) and the other from 17 May 2000 (PHILLS 00). The PHILLS has been under con-

tinual development since 1996 and its characteristics have changed many times as its performance continues to be improved. Likewise, data processing tools for properly accounting for the camera characteristics at the times of these deployments are also in development, and, for historical reasons, the 1999 data scene used in this paper was processed differently than the 2000 scene (Leathers et al. 2001*b*). In both years, there was some contamination of the radiometric data on part of the charge-coupled device (CCD) by light reflected in the camera from the zero-order portion of the diffraction pattern. This artifact was corrected in the 1999 data by flat-fielding the calibrated scenes and corrected in the 2000 scene by modeling and removing the zero-order light from the raw data. Both the focus and the signal-to-noise ratio were improved between 1999 and 2000. Despite these differences in characteristics and calibrations, however, data quality from both years was more than adequate for image classification.

The two PHILLS scenes were atmospherically corrected with the Tafkaa model (Gao et al. 2000). Atmospheric absorption was modeled using concentrations of well-mixed gases typical for tropical areas. The ozone content was set to 0.3 atm-cm, and the water vapor content was set to 1.1 cm in 1999 and 3.5 cm in 2000. The on-ground pixel size was ~1.25 m. Spectral resolution of the raw data was ~4–5 nm and was resampled to every 5 nm from 400–700 nm by a gaussian model. The PHILLS 99 image was warped to match the geometry of the PHILLS 00 image by applying Delauney triangulation warping in ENVI software (Research Systems) with a collection of ground control points.

Algorithm development and results

Our basic approach follows the ordered components outlined in Fig. 1. Bottom reflectance was modeled with three inputs: remote sensing reflectance, bathymetry, and water column attenuation. We developed a bathymetry algorithm for our study site that relied on ratios of remote sensing reflectance. However, this portion of the model is optional and any source of bathymetry can be used. Retrieval of bottom reflectance also required some estimate of water column attenuation. Our method used in situ measurements of the inherent optical properties of the water column, but other methods for remotely estimating water column attenuation can be used as well (*see Discussion*). Retrieved bottom reflectances were then used to derive a quantitative measure of turtlegrass LAI.

Remote sensing reflectance—We compared spectral estimates of R_{rs} measured at the sea surface using the in situ HTSRB with R_{rs} derived from the PHILLS sensor using the 1999 and 2000 datasets (Fig. 3). Field stations corresponding to bright ooitic sand and dense turtlegrass were geolocated in the imagery. In general, R_{rs} derived from the PHILLS sensor captured the overall magnitude and spectral shape of R_{rs} measured with the HTSRB. Some spectral inconsistencies are observed between the two measurements of R_{rs} because the PHILLS was a prototype sensor in its initial development and deployment phase. The PHILLS 99 and 00 tended to overestimate the reflectance in the red region of the spectrum
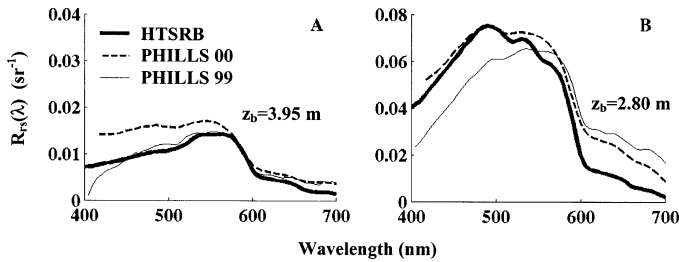
Fig. 3. Remote sensing reflectance spectra, R_{rs}, from the in situ HTSRB instrument, PHILLS 99, and PHILLS 00 for (A) dense seagrass and (B) bright ooitic sand. Water depth, z_b, is shown for each station.

(>660 nm) for both stations. Over dense seagrass, the PHILLS 00 tended to be too bright for most of the spectrum and inflated the blue region of the spectrum (440 nm). Over ooitic sand, the PHILLS 99 data was too low in the blue region. These differences, primarily in the blue and red regions, were due in part to difficulties in atmospheric correction of optically shallow water (Gordon 1997) and calibration issues within the sensors (*see Methods*). Therefore, slight adjustments of the bathymetry and LAI algorithms were required for each year (*see below*). Such corrections should not be necessary as the protocols for calibration, deployment, and atmospheric correction of the PHILLS prototype sensor become further established and its performance continues to improve (Leathers et al. 2001*b*).

Bathymetry—The water-leaving radiance from optically shallow waters was influenced by both bottom reflectance and water depth. Consequently, the retrieval of R_b from R_{rs} requires knowledge of the bathymetry. Previous researchers have mapped water depth by assuming that a pair of wavelength bands can be found such that the ratio of the bottom reflectances in these two bands was the same for all the bottom types within a given scene (Polcyn et al. 1970; Lyzenga 1978). Following this assumption, we developed a site-specific algorithm to map high-resolution bathymetry using reflectance measured with the PHILLS sensor. We exploited the strong absorption of red light by water and the relatively weak absorption of green light to develop a prediction of bathymetry from the ratio of R_{rs} at 555 and 670 nm (Fig. 4A). The second-order polynomial,

$$\log (z_b) = -0.1706x^2 + 0.8913x - 0.2316$$

$$x = \log \left[\frac{R_{rs}(555)}{R_{rs}(670)} \right] \qquad (2)$$

explained >97% of the variation ($p < 0.001$) in water depth (z_b) from HTSRB data collected over eight transects comprised of various mixtures of turtlegrass and sand (Fig. 2C). Approximately 50% of the predictions were within ±0.033 m and the mean residual was ±0.14 m.

Differences in the in situ and remotely sensed spectra, particularly in the red, required adjustment of Eq. 2 for application to the PHILLS data. The corrections followed a simple linear model ($mz_b + b$) with coefficients for PHILLS 99 ($m = 3$, b = -2.97) and PHILLS 00 ($m = 2.67$, b =
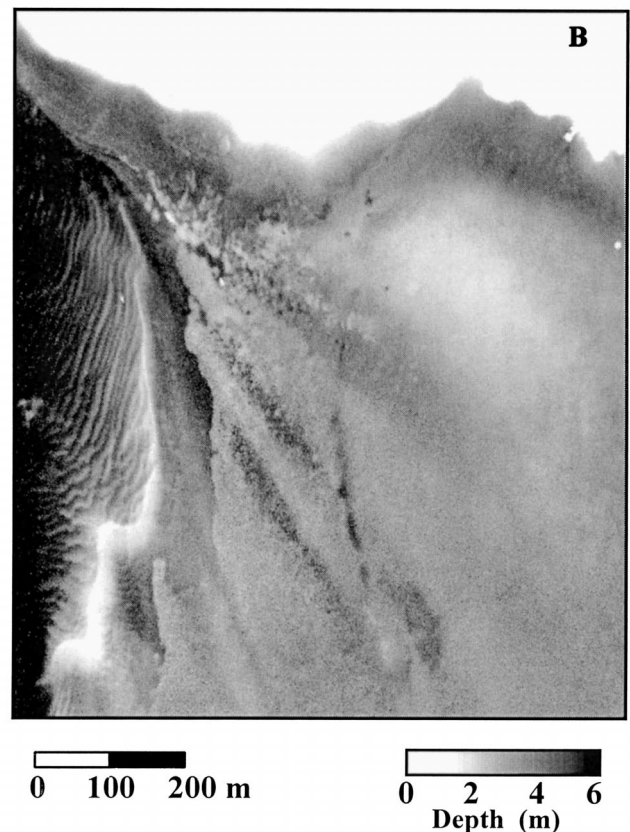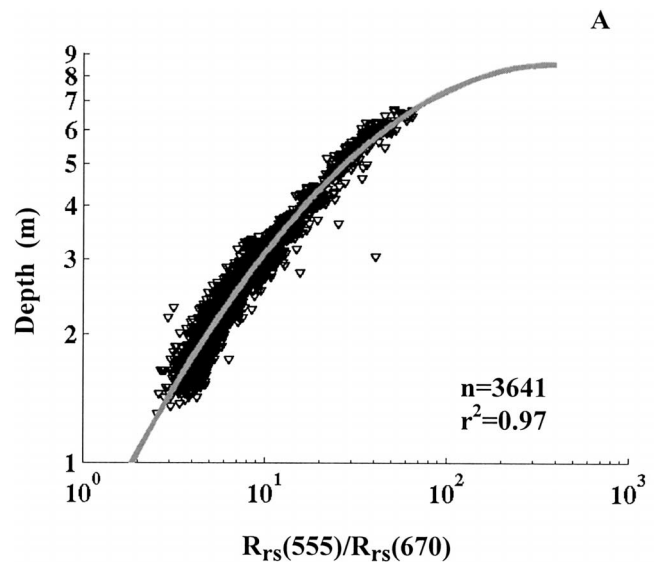

Fig. 4. (A) Relationship between bottom depth and ratio of $R_{rs}(555)/R_{rs}(670)$ (Eq. 2). HTSRB data were collected over transects spanning the study site (Fig. 2). (B) Remotely sensed bathymetry estimated using the PHILLS 99 data.

-2.77). As the calibration and atmospheric correction become more developed for the Ocean PHILLS and other hyperspectral sensors, the in situ and remotely sensed R_{rs} will be more consistent and such spectral corrections will not be necessary.

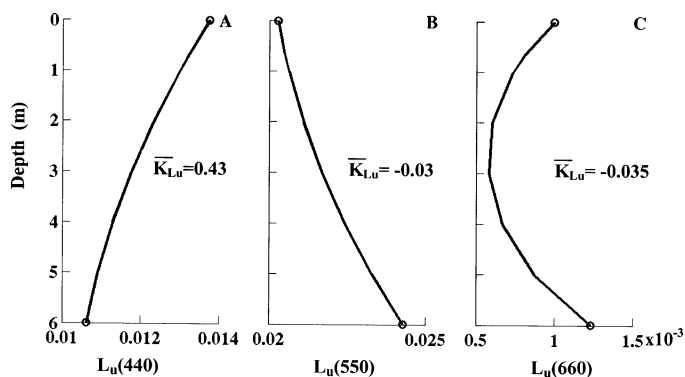A map of bathymetry across the study site was generated

Fig. 5.   Radiative transfer simulations of depth-dependent upwelling radiance modeled at 1-m intervals with a seagrass bottom at 6 m. Depth-averaged upwelling radiance attenuation coefficients, $\bar{K}_{Lu}(z_b)$, were estimated using the two circled points, $L_u(0^-)$ and $L_u(6)$, in each image (Eq. 2). Results are shown for simulations at (A) 440 nm, (B) 550 nm, and (C) 660 nm.

from the PHILLS images by Eq. 2 (Fig. 4B). The map showed considerable structure across the study area throughout the measured depth range of 0–6 m. Important features included a shallow sand bar (emergent at low tide) running through the center of the unvegetated ooid field and detailed sand waves on the west side of the bar in 2–3 m of water. East of the sand bar, the seafloor rose sharply along the boundary between the ooid shoals and the turtlegrass meadow. A series of narrow channels running northwest to southeast created a topography of broad undulating hills in the central portion of the image.

Water column apparent optical properties—In order to determine the relationship between R_{rs} and R_b, the attenuation of E_d and L_u within the water column must be known. Several analytical solutions have been defined to retrieve R_b from reflectance at or just beneath the sea surface (Philpot 1987, 1989; Maritorena et al. 1994). The difficulty in accurately applying these solutions is that attenuation of the upward flux is not equivalent to the attenuation of the downward flux, K_d. Thus, attenuation of the upward flux must be broken down into that originating from the water column and that originating from the bottom (Maritorena et al. 1994). Because the bottom makes the angular structure of the light more isotropic, attenuation of upward flux from the bottom is theoretically always greater than K_d. However, accurate measurement of the K_{Lu} is challenging in optically shallow water. The benthic boundary serves as a source of upwelling photons, particularly for wavelengths not readily absorbed by the bottom (e.g., 550 nm) and alters the apparent attenuation of the upward flux away from the exponential.

As discussed in the Methods section, we used a radiative transfer model to evaluate the distribution of L_u in an optically shallow water column with a dense turtlegrass bottom (Fig. 5). Because the turtlegrass strongly absorbs blue photons, more upwelling photons are produced at the surface than with depth and $\bar{K}_{Lu}(400)$ was positive (Fig. 5A). For the green and red wavelengths (Fig. 5B,C), L_u was greater at the bottom than at the surface and the resulting $\bar{K}_{Lu}(z_b)$ was neg-
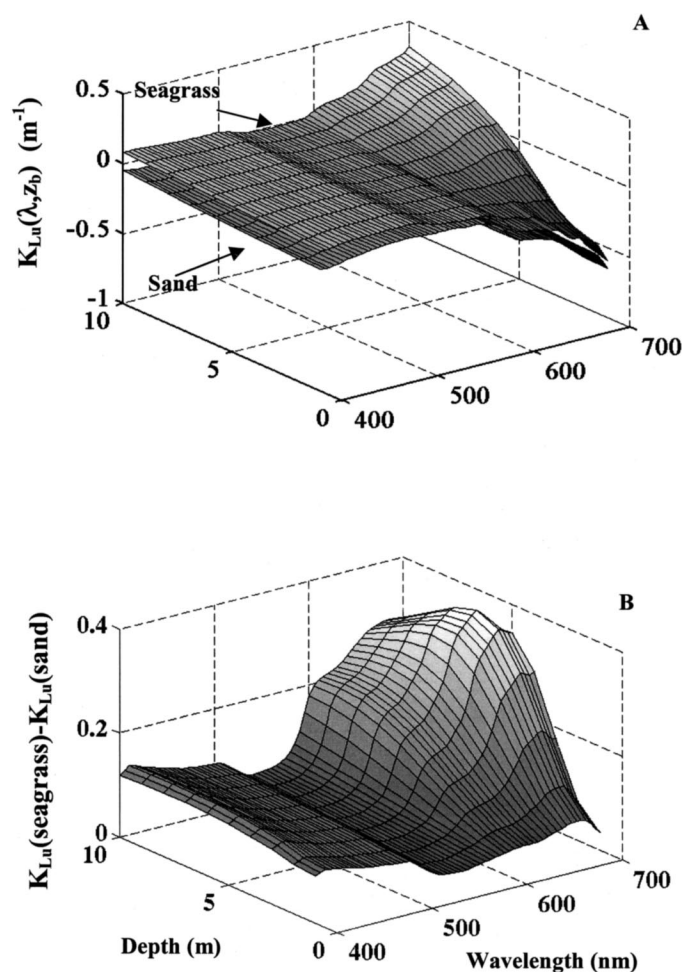

Fig. 6.   (A) $\bar{K}_{Lu}(z_b)$ determined from radiative transfer simulations assuming a bottom comprised of 100% seagrass (upper surface) and sand (lower surface). (B) The difference in modeled $\bar{K}_{Lu}(z_b)$ for a seagrass versus sand bottom.

ative. The vertical profile of $L_u(660)$ (Fig. 5C) curved because water readily absorbs red photons and upwelling radiance was highly attenuated. Although modeled K_d was nearly uniform regardless of water depth, $\bar{K}_{Lu}(z_b)$ was strongly dependent on the bottom depth and was even negative for some wavelengths in optically shallow water.

A $\bar{K}_{Lu}(z_b)$ table was developed from radiative transfer modeling that covered a range of bathymetry from 0 to 10 m (Fig. 6A). For both turtlegrass and sand bottom types, the highest sensitivity to depth was in the red ($>$600 nm), where $\bar{K}_{Lu}(z_b)$ varied from negative values in shallow waters to positive values in deeper waters. $\bar{K}_{Lu}(z_b)$ estimated over sandy bottoms were more negative than over turtlegrass because sand was highly reflective (Fig. 6B). The greatest differences in attenuation over the two different bottom types occurred in the spectral regions that are most absorbed by the seagrass (blue and red). Because the bottom-type is not known a priori when using remote sensing data, our algorithms for estimating turtlegrass LAI (*see below*) focused on the spectral region 530–560 nm where $\bar{K}_{Lu}(z_b)$ varied the least with depth and bottom type ($<$0.07 m^{-1}).
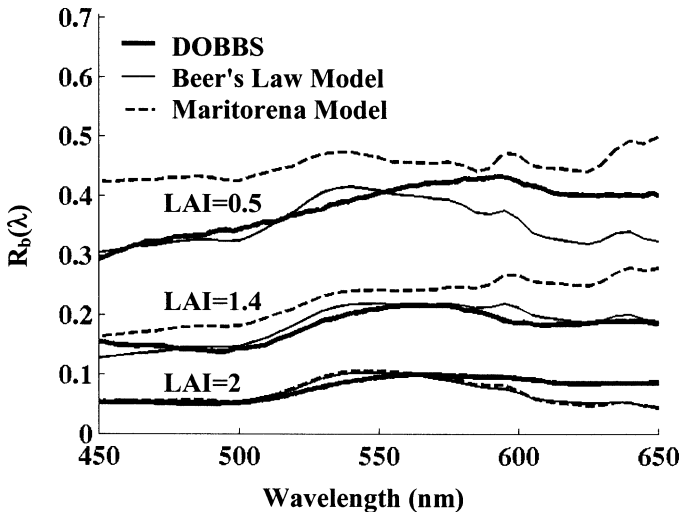
Fig. 7. Bottom reflectance, R_b, measured by the in situ DOBBS instrument and modeled from in situ HTSRB measurements of R_{rs}. The Maritorena model estimated R_b from Eq. 3 and the Beer's Law model from Eq. 5. The three different spectra represent sites with turtlegrass LAI (one-sided leaf area/substrate area) corresponding to dense (LAI = 2), intermediate (LAI = 1.4), and sparse (LAI = 0.5) cover.

Retrieved bottom reflectance—The retrieved bottom reflectance represents the spectral signature of the benthic constituents after removing the distorting influence of the water column. Methods to retrieve R_b from the ocean color measured at the sea surface must take into account the differential absorption and scattering of photons as they pass through the water column both from the surface to the bottom and from the bottom back to the surface. In addition,
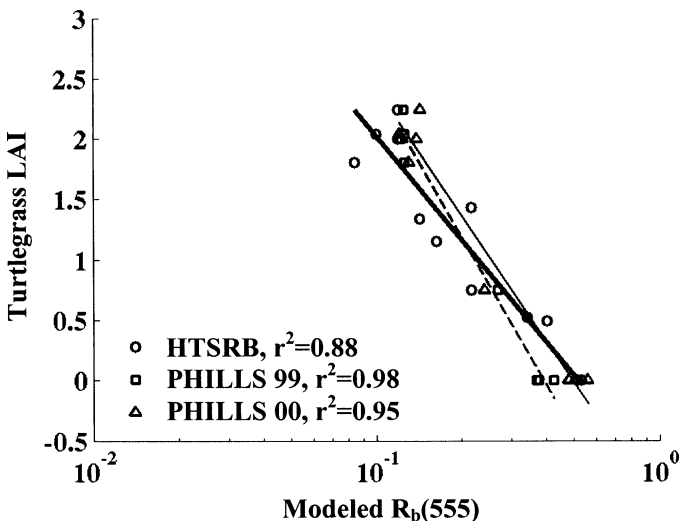

Fig. 8. Relationship between modeled estimates of bottom reflectance $R_b(555)$ and in situ measurements of turtlegrass LAI. R_b was modeled from above-water R_{rs} derived from each instrument. The equation describing each line follows $y = mx + b$, with coefficients for each line as follows: HTSRB ($m = -2.60$, b = -0.69); PHILLS 99 ($m = -3.83$, b = -1.62); and PHILLS 00 ($m = -3.38$, b = -1.06).

the angular distribution of the light fields must be considered because the distribution of downwelling and upwelling photons will be modified by the bottom boundary. We evaluated two methods for retrieving R_b from R_{rs}.

The first method uses the approximate analytical solution to the radiative transfer equation (Maritorena et al. 1994) to retrieve bottom reflectance, R_b, from R_{rs} for water of a given depth (z_b).

$$R_b = R_\infty + (R - R_\infty)\exp(2Kz_b) \qquad (3)$$

$$R = \frac{R_{rs}Q}{t} \qquad (4)$$

R_b was related to reflectance just beneath the sea surface, R, and reflectance measured over an infinitely deep ocean, R_∞. In our approximation, the deep-water R_∞ was estimated by radiative transfer simulations parameterized for the study site. The operational attenuation coefficient, K, represents attenuation of the downwelling stream, and the upwelling stream originating both from the bottom and from the water column (Maritorena et al. 1994). Methods for direct measurement of the operational K are not possible because of the confounding effects of the bottom on the downwelling and upwelling radiation, as shown in Figs. 5, 6. Following Maritorena et al. (1994), K_d was used to represent K because this approximation was found to yield reasonably accurate results in optically shallow waters.

The Maritorena model was developed for reflectance just beneath the sea surface, R, and not R_{rs}. To equal R, R_{rs} must be propagated beneath the sea surface and adjusted by the Q factor, ratio of E_u to L_u (Eq. 4). The transmittance of E_d and L_u up through the air–water interface, t, was approximated as 0.54 (Mobley 1994). According to our radiative transfer simulations, the Q factor just beneath the sea surface was highly dependent on the bottom depth, bottom type, and wavelength. For a 3-m water column overlying a dense seagrass bottom, Q varied spectrally from 2.7 to 3.6. We used the mean Q of 3.2 for this parameterization.

The second method utilized a simple derivation of Beer's Law for retrieving R_b.

$$R_b = \frac{R_{rs}Q_b}{t} \frac{\exp[-\bar{K}_{Lu}(z_b)z_b]}{\exp(-K_d z_b)} \qquad (5)$$

The model was parameterized similarly to Eq. 3. For this model, however, Q_b represents the ratio of E_u to L_u at the bottom interface and was assumed to be π, which is the theoretical value for a Lambertian surface. Measurements of the upwelling radiance distribution over turtlegrass in this region was found to be near-Lambertian at 440 nm (Voss et al. 2003) and R_{rs} is relatively insensitive to non-Lambertian effects (Mobley et al. 2003). The upwelling radiance and downwelling irradiance streams were propagated down to the bottom by the depth-averaged $\bar{K}_{Lu}(z_b)$ and K_d. Values of $\bar{K}_{Lu}(z_b)$ approximated to the nearest meter of z_b were identified from the $\bar{K}_{Lu}(z_b)$ look-up table. Attenuation coefficients at 555 nm were used to map turtlegrass LAI (*see below*): $K_d(555)$ was equal to 0.098 m^{-1} and $\bar{K}_{Lu}(555, z_b)$ ranged from -0.044 m^{-1} at 1 m to -0.011 m^{-1} at 10 m.

Retrieval of R_b using these two models was compared to direct measurements of R_b made with the DOBBS (Fig. 7). The
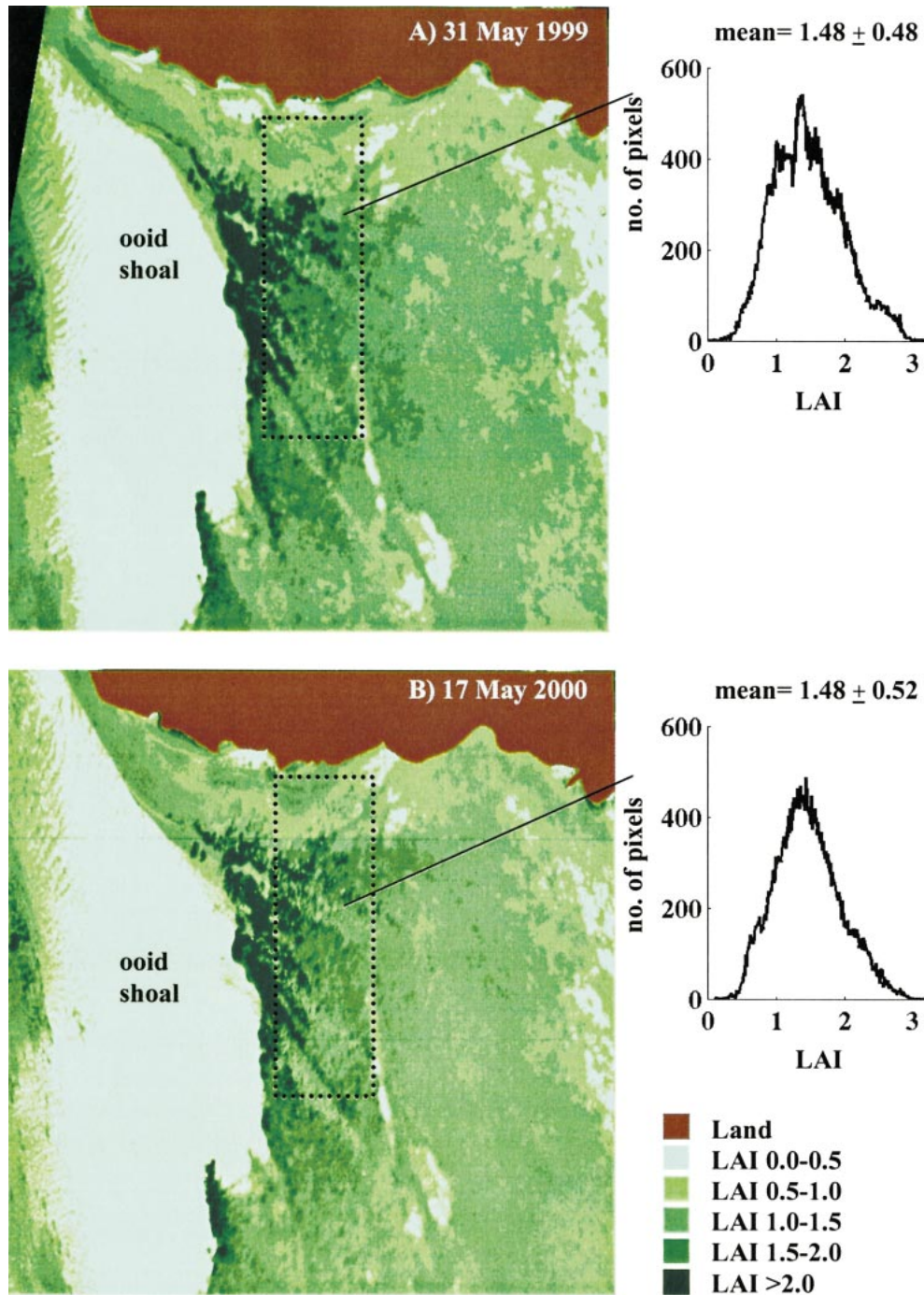
Fig. 9. Distributions of turtlegrass LAI estimated for the study site at Lee Stocking Island, Bahamas, by imagery derived from (A) PHILLS 99 and (B) PHILLS 00. Histograms represent the frequency distribution of LAI within the outlined box of each image.

models were parameterized using surface measurements of R_{rs} from the HTSRB made over sites of dense (LAI = 2), intermediate (LAI = 1.4), and sparse (LAI = 0.5) turtlegrass cover. Measured R_b varied from approximately 10% at 555 nm for dense seagrass to more than 40% for sparse vegetation. For both models, good agreement was found over the dense site. However, the Beer's Law model retrieved more spectrally accurate R_b over intermediate and sparse turtlegrass cover (3–6%

difference). For areas with intermediate and sparse cover, R_b retrieved from the Maritorena formulation significantly overestimated R_b by 20–26% for the entire spectrum, especially at wavelengths greater than 580 nm. Therefore, the Beer's Law model was used in the remainder of this analysis.

Modeled seagrass LAI—We considered a variety of algorithms relating retrieved R_b to LAI (e.g., spectral ratios,

fourth derivative). As LAI increased from 0.49 to 2.0, the absorption in the blue and red increased and R_b decreased to less than 0.10 (Fig. 7). The ratio between $R_b(510)$ and $R_b(530)$ measured in situ with the DOBBS explained 70% of the variability of LAI (data not shown). These wavelengths correspond to the sharp peak in R_b observed over dense turtlegrass vegetation (Fig. 3A). Unfortunately, this peak was not well resolved in the PHILLS data, particularly for the elevated blue spectra in the PHILLS 00 data. Consequently, the magnitude of R_b was the best indicator of the density of turtlegrass. Regression analysis of $R_b(555)$ retrieved with Eq. 5 from both the HTSRB and PHILLS data showed strong correlations between R_b and LAI (Fig. 8). The equation describing each line follows $y = mx + b$ with coefficients for each line as follows: HTSRB ($m = -2.60$, b $= -0.69$); PHILLS 99 ($m = -3.83$, b $= -1.62$); and PHILLS 00 ($m = -3.38$, b $= -1.06$). An analysis of covariance (treatment mean squares [MS] $= 0.243$, error MS $= 0.12$, $F_{2,22} = 2.05$, $p = 0.152$) revealed no significant differences among the HTSRB ($r^2 = 0.88$), PHILLS 99 ($r^2 = 0.98$), and PHILLS 00 ($r^2 = 0.95$) regressions. Spanning nearly an order of magnitude difference in R_b, this relationship was found to be more robust than other models.

Turtlegrass LAI estimated from the PHILLS imagery for both 1999 and 2000 revealed complex spatial patterns across the study site (Fig. 9). The pixels of highest turtlegrass density had LAI > 2 and were found along the boundary with the unvegetated ooid shoals. Bands of intermediate-density turtlegrass (LAI > 1.4) ran along the tops of the broad hills observed in the bathymetry image (cf. Fig. 4B). Interspersed between the dense bands were small sparsely vegetated patches and a long, narrow, sparsely vegetated zone running north–south in both images that corresponded to a narrow deep channel. Histograms of LAI within corresponding regions of the 1999 and 2000 images revealed strikingly similar distributions of turtlegrass (Fig. 9). For both years, LAI within the outlined box was normally distributed about a mean ($\pm$SD) LAI of 1.48 ± 0.5.

Comparisons of turtlegrass LAI (Fig. 9B) with the derived bathymetry (cf. Fig. 4B) revealed that the two algorithms were mapping different spectral features inherent to the imagery. Furthermore, turtlegrass LAI was inversely correlated to the mapped bathymetry, but the resulting relationship was scarcely predictive ($r^2 = 0.6$), and LAI exhibited more fine-scale heterogeneity than the bathymetry (Fig. 10). This inverse correlation further illustrates that bottom type (e.g., turtlegrass, sand) did not significantly affect retrieval of z_b by Eq. 2. The highest densities of seagrass were found on the broad rises near the ooid boundary; the deeper channels were less densely vegetated. However, the turtlegrass distributions varied on meter scales, with both dense and sparse patches in the shallower regions. At 2 m depth, for example, the LAI ranged from <1.5 to >2.5. In contrast, LAI occasionally approached values >1.5 at 4 m.

Discussion

Much of the past research using aerial photography and remote sensing techniques to map seagrass have been limited
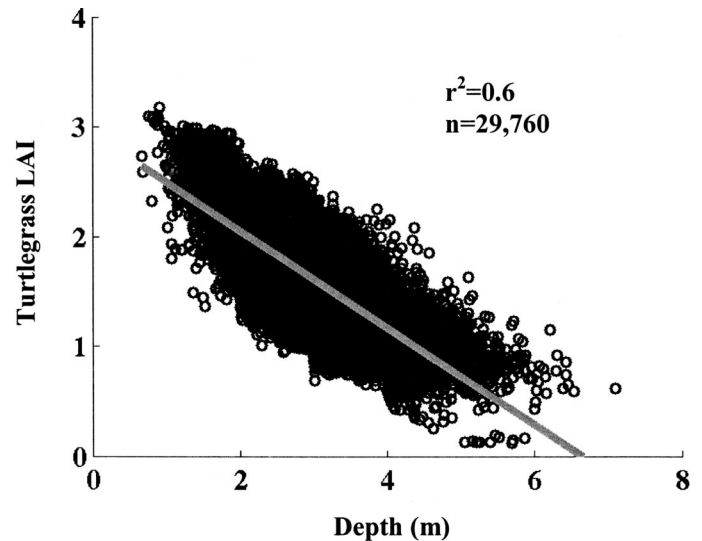
Fig. 10. The relationship between bathymetry and turtlegrass LAI estimated from a central portion of the PHILLS 00 imagery.

to semiquantitative (e.g., percent cover) measures of seagrass abundance (Ferguson et al. 1993; Sheppard et al. 1995; Kirkman 1996). However, absolute quantitative measures, such as LAI, are more useful for estimating ecologically relevant processes, including system productivity. LAI can be converted to standing biomass with simple leaf area–to–mass relationships and can be related to the amount of photosynthesis in the seagrass bed. The algorithm developed here can be used for absolute quantitative estimation of seagrass LAI from digital remote sensing imagery with a precision equivalent to that of ground-based direct counts. The digital nature and extensive areal coverage of remote sensing imagery, however, provide a mechanism for the automated routine creation of high-resolution benthic maps for applications to fundamental ecological studies and the management of coastal resources. Even though this technology is still under development, our analysis has shown that high-resolution ocean color imagery, like the Ocean PHILLS imagery, can be successfully used to map the absolute abundance of submerged vegetation and to evaluate fine-scale spatial and temporal distributions of benthic habitats.

We are currently working to apply this algorithm to spatially and spectrally coarser multichannel satellite data. The relationships developed here focused on spectral regions that are consistent with current multichannel sensors (e.g., SeaWiFS and MODIS). By scaling up our analyses both spatially and spectrally, we can exploit the available long-term remote sensing datasets that have been collected over the last 30 yr and begin to address temporal questions related to stability and climate change. We can also begin to quantify seagrass abundance/density on basin-wide scales and evaluate the role played by submerged aquatic vegetation in global biogeochemical cycles.

A key to developing a remote sensing approach that is generalizable to other regions is to appropriately model the effects of the water column on the bottom reflectance. Therefore, an estimate of bathymetry is needed that is coincident in spatial scale to the remote sensing imagery. Following the

methods of Lyzenga (1978), we developed a site-specific algorithm that can be used to retrieve shallow-water bathymetry from ocean color imagery. However, any bathymetry map could be used in our general approach for quantifying benthic habitats. Our bathymetry equation was specific to the clear waters of the Bahamas Banks, but with appropriate calibration, this simple ratioing technique could prove useful in other sites. The algorithm required that the ratio of a pair of wavelength bands be relatively independent of bottom types within the remotely sensed scene (Lyzenga 1978). Our bathymetry algorithm used the ratio between green reflectance (555 nm), not highly absorbed by most of the benthic vegetation, and red reflectance (670 nm). Although the green/red reflectance ratio was not quite independent of bottom type, no significant differences were observed between the algorithm applied to bottoms comprised of turtlegrass and sand. This is because the green/red reflectance ratio measured at the sea surface is dominated by changes in the red reflectance due to water column attenuation. Red photons are highly attenuated by the water column compared to green photons. Thus, the factor of two difference in the green/red ratio of bottom reflectance between turtlegrass and sand was dwarfed by the order of magnitude differences in water column attenuation between these two wavelengths. The bathymetry algorithm, therefore, was much more sensitive to changes in bottom depth than bottom composition.

Most remote sensing applications assume that negligible amounts of red light leave the water column. In optically shallow water, however, bottom reflectance significantly increases the upward flux of red photons, and measurable amounts of water-leaving radiance can be detected in the red. Our bathymetry algorithm showed an almost linear relationship between depth and the green/red reflectance ratio. However, this function will theoretically asymptote at deeper depths (approximately 8–9 m for this site) when most of the bottom-reflected red light is absorbed by the water column. The depth sensitivity of the algorithm would be reduced in more turbid waters. For sites with large variability in water clarity, a single bathymetry map could be generated from imagery collected under the clearest water conditions and then applied to all other imagery.

The optical signal coming from the benthos is highly modulated by the effects of the water column. Instead of applying the complex radiative transfer equations directly to the entire remotely sensed image (Lee et al. 1994), a simple derivation of Beer's Law combined with a site-specific $\bar{K}_{Lu}(z_b)$ table was used here. The $\bar{K}_{Lu}(z_b)$ table can be built from radiative transfer simulations that include site-specific optical properties and other complex effects (Mobley 1994), such as Raman scattering and fluorescence of chlorophyll and colored dissolved organic materials (the latter not considered for these waters). The $\bar{K}_{Lu}(z_b)$ was developed for bathymetry rounded to the nearest meter and was therefore relatively insensitive to slight differences in bathymetry from tides and turtlegrass canopy height (mean ± SD, 0.22 ± 0.09 m).

For this analysis, we were concerned with modeling turtlegrass densities and applied the $\bar{K}_{Lu}(z_b)$ table determined from turtlegrass to the entire image. Should slight spectral nuances in R_b be required to distinguish benthic components,

then separate $\bar{K}_{Lu}(z_b)$ tables might be required for each bottom type. In that case, an iterative approach could prove useful that (1) applies an average $\bar{K}_{Lu}(z_b)$ table to initially retrieve R_b from all pixels, (2) broadly classifies the image based on the retrieved $R_b(\lambda)$, and (3) recomputes R_b using specific $\bar{K}_{Lu}(z_b)$ tables for different bottom types. Our LAI algorithm, however, was centered on the spectral region (530–550 nm) where the change in bottom type resulted in the lowest differences in $\bar{K}_{Lu}(z_b)$.

The alternative Maritorena model (Eq. 3) was less accurate than the Beer's Law model at retrieving R_b from R_{rs} and consistently overestimated bottom reflectance by 20–26% for all but the densest seagrass bottoms. This model used a single K to represent both upwelling and downwelling attenuation coefficients. In addition, the model was developed for R measured just beneath the sea surface and needed to be adjusted by the factor Q just beneath the sea surface (Eq. 4). However, both parameters Q and K vary spectrally with bottom depth and bottom type. Therefore, application of the Maritorena model would be more accurate with depth- and bottom-specific look-up tables that incorporated the spectral variability in parameters Q and K. The Beer's Law model, however, was parameterized with a single $\bar{K}_{Lu}(z_b)$ look-up table and was more accurate for bottoms comprised of dense, intermediate, and sparse seagrass.

These methods for retrieving R_b from surface reflectance required some knowledge of the water column optical properties. The ultimate objective of remote sensing, however, is to derive all parameters without any in situ measurements. Downwelling attenuation coefficients, for example, could be derived from deep-water pixels and applied to the optically shallow pixels. Empirical algorithms for estimating $K_d(490)$ from remotely sensed reflectance are already employed in multichannel satellite ocean color remote sensing (Austin and Petzold 1981; Mobley 1994; Esaias et al. 1998). In this region, however, the optical properties of shallow water between the islands were typically different from deeper offshore water (E. Boss and R. Zaneveld pers. comm.). Another approach for remotely estimating water attenuation coefficients is to use well-characterized stations within the imagery that have known bottom type and composition. With a priori knowledge of z_b and R_b, the inherent optical properties and resulting water column attenuation can be modeled at these selected stations and then applied to the entire image.

As turtlegrass LAI increased in these waters, both measured and modeled R_b decreased proportionally and LAI was effectively estimated with a simple regression based on $R_b(555)$. Because of our inability to fully correct the prototype PHILLS spectra at all wavelengths, LAI algorithms based on analyses of subtle changes in spectral shape were less accurate than our relatively simple LAI algorithm. Theoretically, the relationship between LAI and modeled $R_b(555)$ would reach a maximum as the bottom reflectance approaches that of 100% seagrass. This could occur either at higher LAI values (>3) or when flow causes the canopy to bend away from the vertical, increasing the horizontally projected LAI (Zimmerman 2003). An important advantage of our two-step approach is that the LAI algorithm is based on retrieved R_b and not surface reflectance or ratios of surface reflectance. This component of the model could be re-

vised independently from the other components to accommodate different types of benthic constituents or shifts in R_b caused by epiphytes, green drift algae, or canopy architecture.

Repeated sampling of the same study site provides a valuable time series that can be used to quantitatively assess changes in benthic habitats. Our analyses of the PHILLS 99 and PHILLS 00 images revealed similar distributions of turtlegrass LAI between the 2 yr. Such consistency would be expected provided that no major disturbances occurred between the sampling interval. However, Hurricane Floyd, a category 4 storm with winds of 135 mph and gusts up to 190 mph, passed through the Bahamas and directly across our study area on 14 September 1999. Although this storm inflicted significant damage to structures on Lee Stocking Island, comparisons of the PHILLS 99 and 00 revealed the turtlegrass distributions in this relatively protected site to be virtually undisturbed. Thus, remote observations allow quantitative exploration of hypotheses related to stability of the benthos and environmental disturbances (Zieman et al. 1988).

In addition to analyzing spatial and temporal patterns, remote sensing imagery is also useful in exploring the mechanistic relationships between spatial distributions and other ecosystem parameters. By comparing distributions of LAI and bathymetry, for example, we can begin to explore the relationship between light availability and turtlegrass distributions and analyze ecological parameters like the maximum-depth distribution. The remotely sensed estimates of turtlegrass LAI were inversely correlated to bathymetry, but the predictive value of this relationship was relatively low ($r^2 = 0.6$). The turtlegrass density varied on a scale of meters or less, whereas the bathymetry was less patchy. The significant correlation between LAI and bottom depth observed here is not surprising given that light availability plays an important role in determining the structure of seagrass ecosystems (reviewed in Duarte 1991). The low predictive value of this relationship, however, suggests that other factors exert significant influences on seagrass distribution in this region. Turtlegrass productivity in oligotrophic waters is largely determined by phosphorus availability (Fourqurean et al. 1992). Thus, the distribution of high turtlegrass densities observed here along the boundary of the ooid shoal could reflect strong gradients in tidal current velocity that promote the transport and deposition of this required nutrient rather than light availability (Jensen et al. 1998).

The use of ocean color remote sensing technology to estimate benthic constituents has been under development for over a decade. The 30-m resolution Landsat thematic mapper (TM) data has been used successfully to estimate submerged vegetation features in shallow waters (Lyzenga 1978; Ackleson and Klemas 1987; Armstrong 1993; Ferguson and Korfmacher 1997; Mumby et al. 1997). However, the high spectral and spatial resolution of the newly emerging remote sensing technology, as demonstrated by the PHILLS sensor, reveals fine-scale variability in the benthos that is useful for mapping seagrass populations that, at first glance, might appear homogeneous. Such fine-scale data can be necessary for evaluating small-scale changes in habitat boundary or

standing crop that often precede catastrophic losses (Mumby et al. 1997).

The application of ocean color remote sensing to quantitative mapping of shallow water habitats is still in its early development, but the ultimate objective is to create algorithms that are robust and applicable to different regions. Our multistep approach permits independent evaluation and modification of individual components without affecting other components of the model. For example, different sources of bathymetry data could be used in the model without changing the remaining components of the model. Differences in water column properties would only modify the input to the equation for retrieving bottom reflectance and would not modify the equations used to retrieve bottom reflectance or to quantify the benthos. Similarly, if the approach was applied to regions with different benthic constituents, then a different model could be applied to quantify the benthos from the retrieved bottom reflectance (e.g., spectral unmixing model to derive percent cover) without substantial modifications to the other components. Future refinements to the algorithms within each component of the model will serve to make each step more robust and portable to different sites.

References

ACKLESON, S. G., AND V. KLEMAS. 1987. Remote sensing of submerged vegetation in lower Chesapeake Bay: A comparison of Landsat MSS to TM imagery. Remote Sens. Environ. **22:** 235–248.

ARMSTRONG, R. A. 1993. Remote sensing of submerged vegetation canopies for biomass estimation. Int. J. Remote Sens. **14:** 621–627.

AUSTIN, R. W., AND T. J. PETZOLD. 1981. The determination of the diffuse attenuation coefficient of sea water using the Coastal Zone Color Scanner, p. 239–256. *In* J. F. R. Gower [ed.], Oceanography from space. Plenum.

CAMBRIDGE, M. L., AND A. J. MCCOMB. 1984. The loss of seagrasses in Cockburn Sound, Western Australia. I. The time course and magnitude of seagrass decline in relation to industrial development. Aquat. Bot. **20:** 229–243.

CAMPBELL, J. B. 1996. Introduction to remote sensing, 2nd ed. Guilford.

DAVIS, C. O., AND OTHERS. 2002. Ocean PHILLS hyperspectral imager: Design, characterization, and calibration. Opt. Express **10:** 210–221.

DUARTE, C. M. 1991. Seagrass depth limits. Aquat. Bot. **40:** 363–377.

ESAIAS, W. E., AND OTHERS. 1998. An overview of MODIS capabilities for ocean science observations. IEEE Trans. Geosci. Remote Sens. **36:** 1250–1265.

FERGUSON, R. L., AND K. KORFMACHER. 1997. Remote sensing and GIS analysis of seagrass meadows in North Carolina, USA. Aquat. Bot, **58:** 241–258.

FERGUSON, R. L., L. L. WOOD, AND D. B. GRAHAM. 1993. Monitoring spatial change in seagrass habitat with aerial photography. Photogramm. Eng. Remote Sens. **59:** 1033–1038.

FOURQUREAN, J., J. ZIEMAN, AND G. POWELL. 1992. Phosphorus limitation of primary production in Florida Bay: Evidence from C:N:P ratios of the dominant seagrass *Thalassia testudinum*. Limnol. Oceanogr. **24:** 1124–1136.

GAO, B. C., M. J. MONTES, Z. AHMAD, AND C. O. DAVIS. 2000. Atmospheric correction algorithm for hyperspectral remote sensing of ocean color from space. Appl. Opt. **39:** 887–896.

GREGG, W., AND K. CARDER. 1990. A simple spectral solar irradiance model for cloudless maritime atmospheres. Limnol. Oceanogr. **35:** 1657–1675.

GORDON, H. R. 1997. Atmospheric correction of ocean color imagery in the Earth Observing System era. J. Geophys. Res. **102:** 17,081–17,106.

HEMMINGA, M., AND C. DUARTE. 2000. Seagrass ecology. Cambridge Univ. Press.

JENSEN, H., K. MCGLATHERY, R. MARINO, AND R. HOWARTH. 1998. Forms and availability of sediment phosphorus in carbonate sand of Bermuda seagrass beds. Limnol. Oceanogr. **43:** 799–810.

KIRKMAN, H. 1996. Baseline and monitoring methods for seagrass meadows. J. Environ. Manage. **47:** 191–201.

LEATHERS, R. A., T. V. DOWNES, AND C. D. MOBLEY. 2001*a*. Self-shading correction for upwelling sea-surface radiance measurements made with buoyed instruments. Opt. Express **8:** 561–570.

LEATHERS, R. A., AND OTHERS. 2001*b*. Ocean PHILLS data collection and processing: Lee Stocking Island, Bahamas, May 2000, Naval Research Laboratory Technical Report NRL/FR/7212-02-10,010.

LEE, Z., AND OTHERS. 1994. Model for the interpretation of hyperspectral remote-sensing reflectance. Appl. Opt. **33:** 5721–5732.

LOUCHARD, E. M., R. P. REID, F. C. STEPHENS, C. O. DAVIS, R. A. LEATHERS, AND T. V. DOWNES. 2003. Optical remote sensing of benthic habitats and bathymetry in coastal environments at Lee Stocking Island, Bahamas: A comparative spectral classification approach. Limnol. Oceanogr. **48:** 511–521.

LYZENGA, D. R. 1978. Passive remote sensing techniques for mapping water depth and bottom features. Appl. Opt. **17:** 379–383.

———. 1981. Remote sensing of bottom reflectance and water attenuation parameters in shallow water using aircraft and Landsat data. Int. J. Remote Sens. **2:** 71–82.

MARITORENA, S., A. MOREL, AND B. GENTILI. 1994. Diffuse reflectance of oceanic shallow waters: Influence of water depth and bottom albedo. Limnol. Oceanogr. **39:** 1689–1703.

MOBLEY, C. D. 1994. Light and water: Radiative transfer in natural waters. Academic.

———, H. ZHANG, AND K. J. VOSS. 2003. Effects of optically shallow bottoms on upwelling radiances: Bidirectional reflectance distribution function effects. Limnol. Oceanogr. **48:** 337–345.

MUMBY, P. J., E. P. GREEN, A. J. EDWARDS, AND C. D. CLARK. 1997. Measurement of seagrass standing crop using satellite and digital airborne remote sensing. Mar. Ecol. Prog. Ser. **159:** 51–60.

ORTH, R., AND K. MOORE. 1983. Chesapeake Bay: An unprecedented decline in submerged aquatic vegetation. Science **222:** 51–53.

———. 1977. Effect of nutrient enrichment on growth of the eelgrass *Zostera marina* in the Chesapeake Bay, Virginia, USA. Mar. Biol. **44:** 187–194.

PETERSON, B. J., AND J. W. FOURQREAN. 2001. Large-scale patterns in seagrass (*Thalassia testudinum*) demographic in south Florida. Limnol. Oceanogr. **46:** 1077–1090.

PHILPOT, W. D. 1987. Radiative transfer in stratified waters: A single-scattering approximation for irradiance. Appl. Opt. **26:** 4123–4132.

———. 1989. Bathymetric mapping with passive multispectral imagery. Appl. Opt. **28:** 1569–1578.

POLCYN, F. C., W. L. BROWN, AND I. J. SATTINGER. 1970. The measurement of water depth by remote sensing techniques. The University of Michigan, Ann Arbor, Willow Run Laboratories Report 8973-26F. 8973-26F.

SHEPPARD, C. R. C., AND OTHERS. 1995. Habitat mapping in the Caribbean for management and conservation: Use and assessment of aerial photography. Aquat. Conserv. Mar. Freshw. Ecosyst. **5:** 277–298.

VALIELA, I., AND OTHERS. 1992. Couplings of watersheds and coastal waters: Sources and consequences of nutrient enrichment in Waiquoit Bay, Massachusetts. Estuaries **15:** 443–457.

VOSS, K. J., C. D. MOBLEY, L. K. SUNDMAN, J. IVEY, AND C. MAZELL. 2003. The spectral upwelling radiance distribution in optically shallow waters. Limnol. Oceanogr. **48:** 364–373.

ZIEMAN, J., AND OTHERS. 1988. A catastrophic die-off of seagrasses in Florida Bay and Everglades National Park: Extent, effect and potential causes. Eos **69:** 111.

ZIMMERMAN, R. 2003. A biooptical model of irradiance distribution and photosynthesis in seagrass canopies. Limnol. Oceanogr. **48:** 568–585